ARTICLE

Controlled composite processing based on off-stoichiometric thiol-epoxy dual-curing systems with sequential heat release (SHR)

Albert Fabregat-Sanjuan[1] | Xavier Fernández-Francos[2] 🔵 | Francesc Ferrando-Piera[1]

[1]Mechanical Engineering Department, Universitat Rovira i Virgili, Tarragona, Spain

[2]Thermodynamics Laboratory, ETSEIB, Universitat Politècnica de Catalunya, Barcelona, Spain

Correspondence
Xavier Fernández-Francos, Thermodynamics Laboratory, ETSEIB, Universitat Politècnica de Catalunya, Av. Diagonal 647, Barcelona 08028, Spain.
Email: xavier.fernandez@upc.edu

Abstract

Control of curing rate and exothermicity during processing of thermosetting composite materials is essential in order to minimize the formation of internal stresses leading to mechanical and dimensional defects in the samples, especially in thick composite samples. It was recently proposed that sequential heat release, an approach based on the kinetic control of the curing sequence of dual-curing thermosets, would enable a step-wise release of the reaction heat and therefore a better control of conversion and temperature profiles during the crosslinking stage. In this article, it is shown experimental proof of this concept obtained by means of an instrumented mold that can be used for the processing of small samples with and without carbon fiber reinforcement. Safe processing scenarios have been defined by numerical simulation using a simplified two-dimensional heat transfer model and validated experimentally.

KEYWORDS
composites, kinetics, structure-property relationships, thermal properties, thermosets

1 | INTRODUCTION

Control of temperature-conversion profiles during processing of thermoset components is essential in order to minimize the formation of internal stresses leading to a number of mechanical and dimensional defects.[1,2] To that end, a number of optimization strategies have been proposed, based on goal functions aimed at reducing the temperature overshoot and conversion gap between composite layers or internal stresses, optimization of processing time and maximization of the degree of cure.[1–7]

It was recently proposed the use of a different approach based on the sequential heat release (SHR), taking place in the processing of dual-curing systems with controlled curing sequence.[8] Sequential dual-curing systems[9] make it possible to obtain a stable intermediate material with a controlled network structure and properties after the first curing stage, leading to the ultimate material after the activation of the second curing stage. For the intended application, the control of the curing sequence and therefore the exothermic behavior is of high interest to prevent the occurrence of uncontrolled temperature overshoots and non-uniform curing profiles. The simulation results using a dual-curing test formulation based on off-stoichiometric thiol-epoxy chemistry[8] showed that it was very easy to achieve an intermediate material with uniform conversion thanks to the self-limiting character of the first reaction. A suitable trial-

and-error choice of first stage temperature made it possible to control the temperature overshoot caused by the first reaction and therefore prevent premature activation of the second reaction, which had substantially slower kinetics. In addition, it was found that a simple numerical optimization of first stage dwell time and second stage heating rate was sufficient to obtain controlled and uniform conversion profiles and limited temperature overshoot in the crosslinking process after the gel point. Processing based on a dual-curing reaction scheme is therefore not subject to tight time–temperature processing constraints, unlike conventional B-stage processing,[2,10] and complex algorithms[1-3] may not be required in order to define near-optimal temperature programs. Nevertheless, they could be subject to further optimization by means of different procedures such as Pareto-based optimization.[8] However, no experimental evidence of the validity of this concept was provided.

In the present work the temperature and conversion profiles obtained during processing of composites based on dual-curable off-stoichiometric thiol-epoxy formulations are analyzed, and compared with the simulation of the curing process. To that end, a low-cost experimental device has been designed and built in order to analyze the vacuum-assisted resin transfer molding (VARTM) processing of small composite parts.[11] The device is capable of programming curing schedules with controlled heating rate, temperature steps and dwell times on one side or both sides of the composite. The instrumentation of the device allows to monitor the interior of the composite, mold plates and environment temperatures. Monitoring and control of the process is based on an Arduino™ platform. The device has been designed for the processing of 5 cm diameter composite parts with thickness of 6 or 15 mm. The cylindrical geometry has been chosen in order to facilitate simulation by transformation of a three-dimensional (3D) system into a two-dimensional (2D) system with cylindrical symmetry. The geometrical design and digital manufacturing of the device has been performed with Autodesk™. Simulation of the curing stage of the VARTM process has been performed with MATLAB™ using a simplified 2D geometrical model, an approximation that was validated by comparison with steady state simulation of the exact 3D model with Autodesk.[11] A dual-curing resin formulation similar to the one employed in a previous work has been used.[8] The curing kinetics and thermophysical properties of the resin have been studied by thermal analysis techniques and modeled conveniently for the simulation. Thermophysical properties of the mold components have been determined from literature data. The effect of sample thickness, the use of carbon fiber (CF) as filler and the heating program has been studied.

2 | MATERIALS AND METHODS

2.1 | Experimental VARTM equipment

A low-cost experimental VARTM device has been built in order to study test formulations using a reduced amount of material. A complete description of the device has been published elsewhere.[11] The components of the mold are shown in Figure 1. The mold has been designed with cylindrical geometry in order to facilitate comparison of experimental and simulation results. The resin/composite diameter has been set to 5 cm, with a thickness of 6.6 or 15.2 mm being controlled by the Teflon ring. Total diameter of the aluminum plate and Teflon ring is 11 cm. The thickness of the aluminum plate is 5 mm, the insulation thickness employed is of 17 mm and the PLA case is 1.5 mm thick. Main dimension can also be appreciated in Figure 1. Aluminum has been chosen as material for the upper and lower heating plates in order to achieve proper heat distribution in the radial direction ensuring one-dimensional heat flow conditions within the resin. In addition to the components identified in Figure 1, it can be observed the presence of a resin feed inlet across the upper case, insulation and plate elements, and an outlet across the lower case, insulation and plate for the application of vacuum inside the mold to produce the infusion of the resin into the mold cavity. The aluminum plates and the Teflon ring are bolted, and rubber gaskets are placed between the Teflon ring and the upper and lower aluminum plates in order to ensure good sealing during vacuum infusion and processing. Although it is not specified in the figure, the lower aluminum plate can also be equipped with a second heating element in order to enable symmetrical upper and lower boundary conditions. Figure 2 shows an image of the real mold without the upper case and insulation.

The upper and lower aluminum plates are instrumented with Platinum Resistance Temperature Detectors (RTD) sensors (PT1000) for temperature monitoring and control. Negative temperature coefficient (NTC) probes are used to monitor the resin temperature in the middle of the composite part and another one to monitor the environment temperature. The heating element has a maximum power of 13 W, is adhered to the aluminum plates and the power is controlled by means of a power MOFSET enabling a pulse-width-modulating (PWM) signal for a smooth PID control. The monitorization of the system temperatures and the control of the heating program via the heating elements is based on an Arduino Uno™ micro-controller together with Adafruit MAX31865 amplifiers for PT1000 probes. The communication interface is based on module PLX-DAQ v2 enabling configuration of the interface using VBA code in Excel™. NTC probes are previously calibrated using the
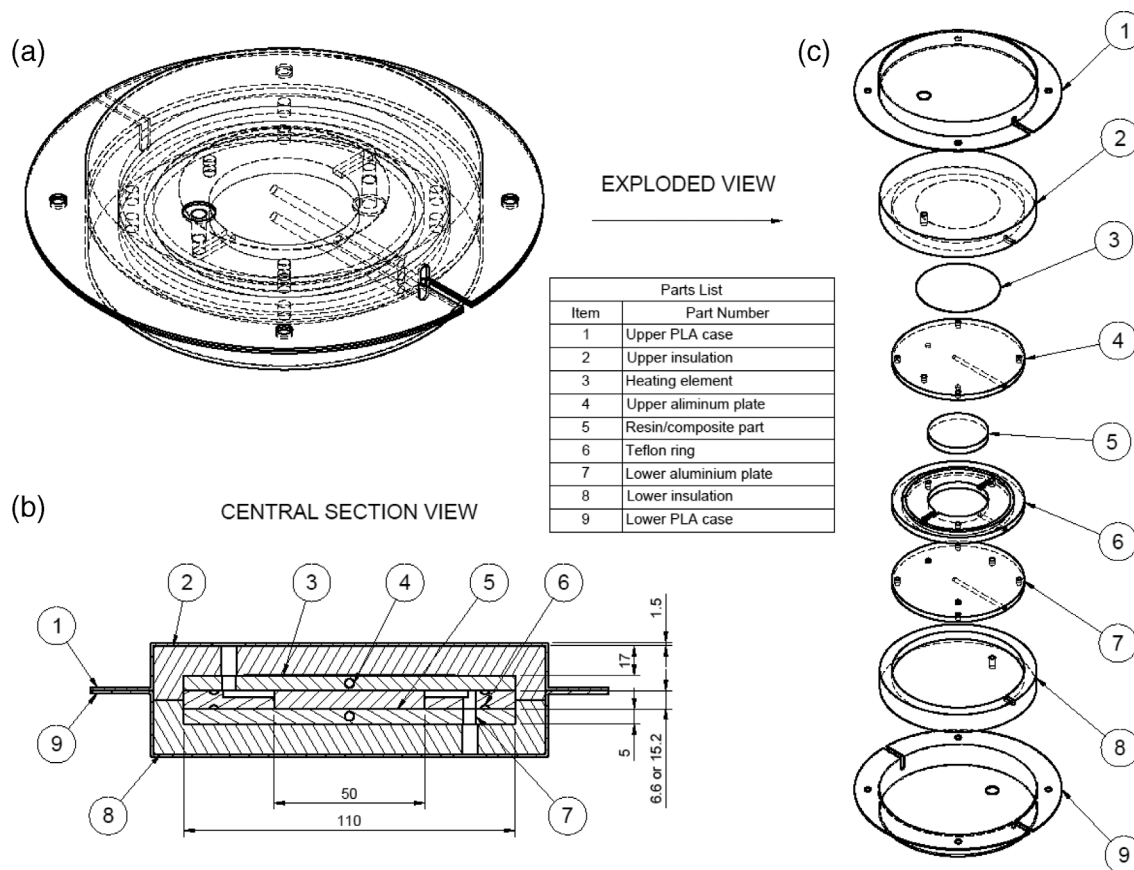
FIGURE 1 Components of the experimental device for VARTM processing with a single heating element: (a) isometric view of the assembly with interior geometry viewed by dashed lines, (b) cross-section view with main dimensions, and (c) exploded view

PT1000 probes as reference in an aluminum block for a temperature range higher than the used in the VARTM device.

2.2 | Materials

2.2.1 | Resin and composite parts

A diglycidyl ether of Bisphenol A epoxy resin (tradename EBL70, Po. int. Er. S.r.l., Torino, Italy) coded as DG, with an equivalent weight of 184.5 g per epoxy group was used. Pentaerythritol tetrakis (3-mercaptopropionate) (489 g/mol, Sigma-Aldrich), coded as S4, was used as a thiol crosslinking agent. 1-methylimidazole (82 g/mol, Sigma-Aldrich), coded as 1MI, was used as anionic initiator for the epoxy-thiol addition and excess epoxy homopolymerization. DG was dried under vacuum at 80°C for 2 h prior to use. The other reagents were used as received.

An off-stoichiometric thiol-epoxy formulation with excess epoxy groups, DGS4-0.45 was prepared by mixing 77.2 wt% of DG and 22.8 wt% of S4, yielding a formulation with a molar ratio of thiol groups to epoxy groups of 0.45:1 approximately. 1 phr of 1MI was finally added immediately before use.

Carbon Fiber Cloth Fabric 12 k 2/2 Twill, of 650 g/m^2, manufactured by Mitsubishi (Grafil™ 34–700 12 K), was supplied by EasyComposites (Stoke-on-Trent, UK).

2.2.2 | VARTM experimental setup

Teflon and open-cell polyurethane foam were supplied by Industria de la Goma S.A. (Tarragona, Spain). Aluminum alloy EN AW 2024 was supplied by LUMETAL Plastic (Sant Boi de Llobregat, Spain). PT1000 sensors and amplifiers for the monitoring of the upper and lower plate temperatures were purchased from Adafruit (New York). Heating elements, pneumatic fittings, the Arduino kit components, thermistors and other minor electronic components were purchased from RS Amidata (Madrid, Spain). Resin feed plastic tubes were purchased from EasyComposites (Stoke-on-Trent, UK). Demolding wax was purchased from Feroca (Madrid, Spain). The Teflon ring and aluminum plates have been manufactured using
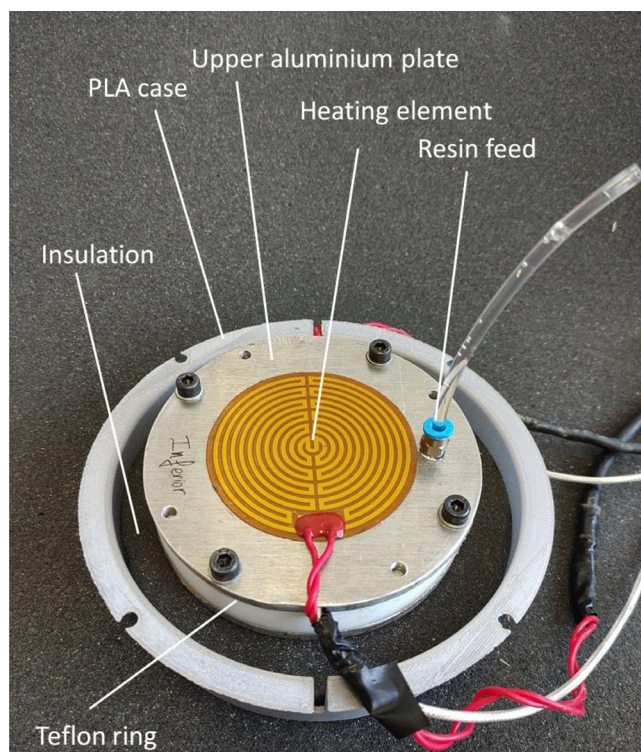
FIGURE 2   Upper view of the experimental setup without the upper PLA case and insulation, showing the fitting of the resin feed tube [Color figure can be viewed at wileyonlinelibrary.com]

the computer assisted manufacturing (CAM) module from Fusion 360 (Autodesk) and machined with a multi-purpose BoXZY desktop machine. The CF has been die-cut to suitable size to fit the mold cavity.

2.3 | VARTM processing

The DGS4-0.45 mixture was prepared 1 day before utilization in the VARTM setup: the DG and S4 components were mixed and homogenized by hand stirring using a spatula for 5 min and degassed at 50°C under vacuum for 2 h. Before the experiment, 1MI was added to the DGS4 mixture and homogenized by hand stirring using a spatula for 5 min, followed by a degassing at room temperature for 15 min. Vacuum was created inside the VARTM mold prior to infusion of the resin. When CF reinforced samples were prepared, different layers of the clothing were die-cut and placed inside the mold before infusion. The CF volume fraction was calculated after the experiments taking into consideration the weight of CF clothing used and the total sample weight, fiber and resin densities and the dimensions of the mold.

Programmed temperature schedules consisted on five steps:

1. Heating at 1–2.5 °C/min from room temperature to the first dwell temperature of 40 °C,
2. Isothermal dwell at 40°C for 60–80 min,
3. A second heating at 1–2.5°C/min up to the second dwell temperature of 80°C,
4. Isothermal dwell at 80°C for 60–80 min, and
5. Cooling down to room temperature by convective heat dissipation with the environment.

The choice of different heating rates depended on the use of a single heating element (1°C/min) or two heating elements (2.5°C/min), one on the upper plate and the other on the lower plate.

2.4 | Thermal analysis

The curing kinetics and the thermal properties were analyzed using differential scanning calorimetry (DSC). A Mettler DSC 3+ equipped with an intra-cooler and a DSC822e equipped with a sampling robot and cooled with liquid nitrogen were used. Both devices were calibrated using Indium and Zinc standards.

The curing stages of DGS4-0.45 formulations were analyzed independently. The first curing reaction was analyzed at different heating rates β ranging from 1.25 to 20°C/min and isothermally at temperatures T between 20 and 80°C. The second curing reaction was analyzed after a pre-curing step at 80°C for 5 min to complete the first reaction, at heating rates β between 1.25 and 10°C/min and isothermally at T between 90 and 130°C.

The degree of conversion x and the reaction rate dx/dt were determined using the following expressions:

$$x = \frac{\Delta h}{\Delta h_{\text{total}}} \quad \frac{dx}{dt} = \frac{dh/dt}{\Delta h_{\text{total}}} \tag{1}$$

Where Δh is the heat released up to a time t (isothermal curing) or temperature T (dynamic curing), dh/dt is the instantaneous heat flow and Δh_{total} is the total heat evolved in the curing process, assuming complete cure. For the first curing process, $\Delta h_{total,1}$ was determined as an average value from the integration of the isothermal and non-isothermal experiments up to the end of the first curing process. For the second curing process, $\Delta h_{total,2}$ was calculated as an average value from the integration of the non-isothermal experiments after the pre-cure of the samples.

The specific heat capacity c_P was determined according to method DIN 51007 using alumina (Al_2O_3) as reference substance.[12] The density ρ of the samples was assumed to be constant and was determined from simple mixing rules taking into account the density of the

individual components of the formulation. The thermal conductivity λ of the uncured and cured resin was not measured and it was assumed to be constant and similar to the one of previously studied stoichiometric and off-stoichiometric thiol-epoxy materials.[8,13]

The glass transition temperature T_g was determined using DSC at a heating rate of $10\,^\circ C/min$ as the halfway point in the heat capacity step Δc_P. Measurements were done before curing (T_{g0} and Δc_{P0}), after the first curing stage (T_{gint} and Δc_{Pint}) and at the end of the curing process ($T_{g\infty}$ and $\Delta c_{P\infty}$). The glass transition temperature-conversion relationship $T_g(x)$ was determined independently for the first and second curing stages[8] making use of the Venditti and Gillham expression[14]:

$$\ln T_{g,1}(x_1) = \frac{(1-x_1)\cdot \ln T_{g0} + (\Delta c_{Pint}/\Delta c_{P0})\cdot x_1 \cdot \ln T_{gint}}{(1-x_1)+(\Delta c_{Pint}/\Delta c_{P0})\cdot x_1}$$
$$\ln T_{g,2}(x_2) = \frac{(1-x_2)\cdot \ln T_{gint} + (\Delta c_{P\infty}/\Delta c_{Pint})\cdot x_2 \cdot \ln T_{g\infty}}{(1-x_2)+(\Delta c_{P\infty}/\Delta c_{Pintt})\cdot x_2} \quad (2)$$

where $T_{g,1}(x_1)$ represents the glass transition temperature in the first curing process, with conversion x_1, and $T_{g,2}(x_2)$ is the glass transition temperature in the second curing process, with conversion x_2.

2.5 | Kinetics analysis

The curing kinetics have been modeled using a kinetic model based on multiple elements in parallel[8] with a pseudo-induction period in order to model the start of the reaction. The induction period has been modeled in the following manner:

$$\frac{dx}{dt} = x_{ind}\frac{\exp(-E_{ind}/R\cdot T)}{g(x_{ind})/k_{0,ind}} x < x_{ind} \quad (3)$$

where x_{ind} is the degree of conversion associated with this induction period, which has been set to 0.01. Parameters E_{ind} y $g(x_{ind})/k_{0,ind}$ have been determined for $x = x_{ind} = 0.01$ by means of a non-linear isoconversional integral analysis making use of dynamic and isothermal data, as in our previous work.[8] After the induction period, the curing has been modeled using the following expressions:

$$\frac{dx}{dt} = \sum k_i \cdot (1-x)^{n_i} \cdot x^{m_i} \ x \geq x_{ind} \quad (4)$$

where k_i is a rate constant with an Arrhenius temperature dependence $k_i = k_{0,i}\cdot \exp(-E_i/R\cdot T)$, with activation energy E_i and preexponential factor $k_{0,i}$; n_i and m_i are the apparent reaction orders of the autocatalytic element.

The kinetic parameters have been determined by means of multivariate non-linear regression starting from experimental reaction rate obtained under isothermal and non-isothermal conditions.

2.6 | Simulation

Taking into account the slow start of the thiol-epoxy reaction, and following our previous work[8] it was decided to simulate only curing stage of the VARTM processing in the experimental setup, neglecting the mold filling stage.

2.6.1 | Simulation geometry

The mold is a tridimensional element but the cylindrical geometry (Figure 1) made it possible to assume a simplified scenario with two-dimensional heat transfer conditions with cylindrical symmetry, as illustrated in Figure 3.

2.6.2 | Simulation model

The general equation for the two-dimensional heat transfer with cylindrical coordinates is:

$$\frac{1}{r}\cdot\frac{d}{dr}\left(\lambda\cdot r\cdot\frac{dT}{dr}\right)+\frac{d}{dz}\left(\lambda\cdot\frac{dT}{dz}\right)+q_{gen}=\rho\cdot c_p\cdot\frac{dT}{dt} \quad (5)$$

where λ, ρ and c_p are the effective termal conductivity, the density and the specific heat capacity, respectively, and T is the temperature. The axial direction is represented by z and the radial direction is given by r. q_{gen} is the heat generation per unit volume and is only present in the heating element and the resin/composite. Discretization is made with variable Δz and Δr in the z and r directions, respectively, in order to adapt to the dimensions of the different components. Properties of the materials are diverse in different zones to model the heat transfer properly.

Figure 3a shows a simplified representation of the mold with the studied section, and Figure 3b shows a characteristic finite element with discrete length Δz and Δr in the axial and radial directions, respectively. Figure 3c shows the different regions in the simulation section corresponding to the scenario in which there is a single heating element, in which there is only symmetry with respect to the z axis. In contrast, when a second heating element is added to the lower plate, additional symmetry in the central plane can be considered, leading to the representation of the simulation section of
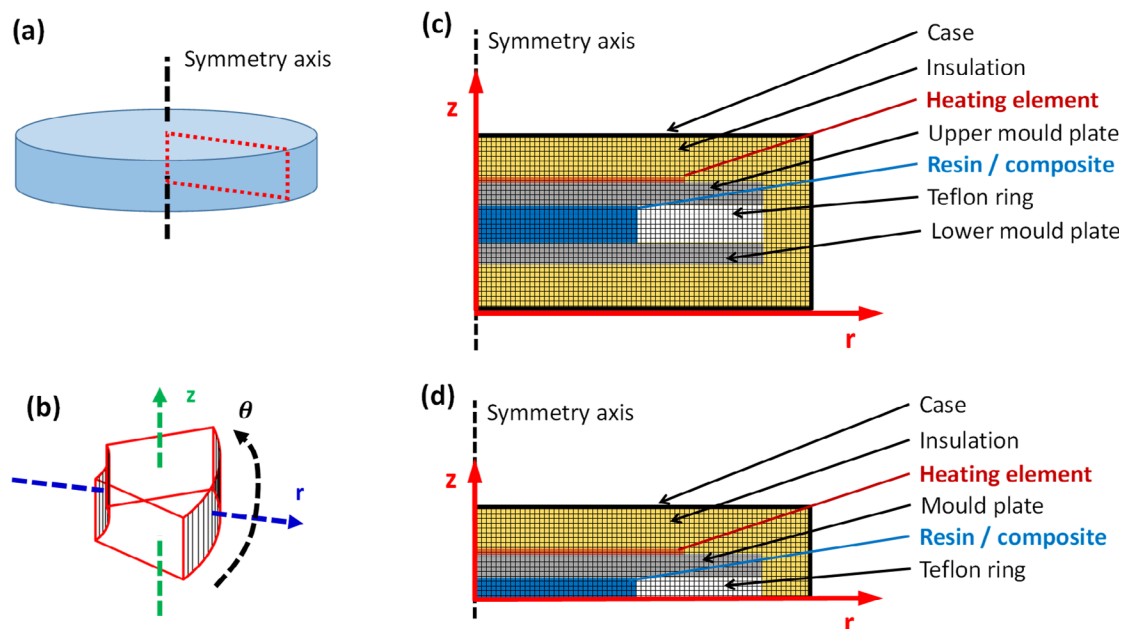
FIGURE 3 Schematics of the VARTM mold for the simulation under two-dimensional heat transfer with cylindrical symmetry: (a) overall representation of the mold with highlighted two-dimensional simulation section, (b) discrete element analyzed in the simulation, (c) two-dimensional simulation section for the mold with upper heating and (d) two-dimensional simulation section with heating on both sides, with symmetry in the middle plane [Color figure can be viewed at wileyonlinelibrary.com]

Figure 3d. This latter configuration will be preferred because it will enable the use of higher heating rates, as will be seen later, and speed up the simulation process.

In the case of the heat generation by the curing reaction:

$$q_{gen} = \frac{dh}{dt} \cdot \phi_r \cdot \rho_r \tag{6}$$

Where dh/dt is the heat flow generated per unit mass, ϕ_r is the resin volume fraction and ρ_r is the resin density. In this dual-curing system, the heat flow can be expressed as:

$$\frac{dh}{dt} = \Delta h_{total,1} \cdot \frac{dx_1}{dt} + \Delta h_{total,2} \cdot \frac{dx_2}{dt} \tag{7}$$

Where the subscripts 1 and 2 indicate the first and second curing process, respectively. It can also be assumed that the dual-curing system is strictly sequential, and therefore the second process only starts when the first one is finished.[8] A global conversion epoxy groups, x_{epoxy}, is determined as:

$$x_{epoxy} = f_{thiol} \cdot x_1 + (1 - f_{thiol}) \cdot x_2 \tag{8}$$

Where $f_{thiol} = 0.45$ is the ratio between thiol and epoxy groups in the formulation. Assuming that the curing process is strictly sequential, in the first stage of the curing process it can be assumed that $x_{epoxy} = f_{thiol} \cdot x_1$, and in the second stage $x_{epoxy} = f_{thiol} + (1 - f_{thiol}) \cdot x_2$. Rate of epoxy group conversion is in consequence calculated as

$$\frac{dx_{epoxy}}{dt} = f_{thiol} \cdot \frac{dx_1}{dt} + (1 - f_{thiol}) \cdot \frac{dx_2}{dt} \tag{9}$$

Following the same line of reasoning, in the first stage of the curing process it can be assumed that $dx_2/dt = 0$ and $dx_{epoxy}/dt = f_{thiol} \cdot dx_1/dt$, and in the second stage $dx_1/dt = 0$ and $dx_{epoxy}/dt = (1 - f_{thiol}) \cdot dx_2/dt$. However, from a practical point of view, it has been allowed the second reaction to start when $x_1 = 0.99$.

In the case of the heating element, it has been used a q_{gen} with a maximum value of 0.011 W/mm³ taking into account the dimension and the maximum power, and it is only activated according to the prescribed temperature program.

Different boundary conditions were established in the simulation. In the symmetry axis, $r = 0$, it was assumed adiabatic behavior, $dT/dr = 0$. In the outermost layer, $r = r_{max}$, the boundary condition was set as:

$$\lambda \cdot \frac{dT}{dr} = h_{rad-conv} \cdot (T_{env} - T_{r=r_{max}}) \tag{10}$$

Where T_{env} is the environment temperature, $T_{r=r_{max}}$ is the surface temperature and $h_{rad-conv}$ is a convection-radiation coefficient calculated as:

$$h_{rad-conv} = h_{conv} + \sigma \cdot \varepsilon \cdot \frac{(T_{env}^4 - T_{r=r_{max}}^4)}{T_{env} - T_{r=r_{max}}} \qquad (11)$$

Where h_{conv} corresponds to the convection coefficient of the air surrounding the device, σ is the Steffan-Boltzmann constant, ε is the emissivity of the mold temperature and T_{env} is the temperature of the room walls surrounding the device and assumed equal to the environment temperature. It was also assumed that $h_{conv} = 5\,W/m^2 \cdot K$, $\sigma = 5.6704 \cdot 10^{-8}\,W/m^2 \cdot K^4$, $\varepsilon = 0.9$. Both T_{env} and $T_{r=r_{max}}$ are expressed in K in the previous expression. In the absence of the environment temperature monitorization, it was assumed to be equal to the initial mold temperature.

For the surfaces with $z = z_{max}$ and $z = 0$, the boundary conditions were established as:

$$\lambda \cdot \frac{dT}{dz} = h_{rad-conv} \cdot (T_{env} - T_{z=z_{max}}) \qquad (12)$$

$$\lambda \cdot \frac{dT}{dz} = -h_{rad-conv} \cdot (T_{env} - T_{z=0}) \qquad (13)$$

Where $T_{z=z_{max}}$ and $T_{z=0}$ are the upper and lower surface temperatures, respectively, and $h_{rad-conv}$ is determined as in the previous case, depending on the surface temperature. In the case of the symmetrical mold, with two heating elements, only half of the mold was simulated and, in this case, an adiabatic boundary was considered for $z = 0$, $dT/dz = 0$.

The simulation was carried out using MATLAB by means of a home-made algorithm for the numerical integration of the heat equation based on the implicit solution of the nodal temperatures making use of the alternating differences method, in a similar way to other works.[15] The general heat diffusion equation was conveniently transformed into a general equation as:

$$\begin{aligned} U_{z+}^{i,j} \cdot T^{i,j+1} + U_{z-}^{i,j} \cdot T^{i,j-1} + U_{r+}^{i,j} \cdot T^{i+1,j} + U_{r-}^{i,j} \cdot T^{i-1,j} \\ - \left(U_{z+}^{i,j} + U_{z-}^{i,j} + U_{r+}^{i,j} + U_{r-}^{i,j} \right) \cdot T^{i,j} + \frac{q_{gen}}{\rho \cdot c_p} \\ = \frac{dT^{i,j}}{dt} \end{aligned} \qquad (14)$$

Where i,j represent the node positions in the r and z directions respectively, $U_{z+}^{i,j}$, $U_{z-}^{i,j}$, $U_{r+}^{i,j}$ and $U_{r-}^{i,j}$ are coefficients that represent the contribution to temperature change by heat transfer with up and down (z direction), and exterior and interior (r direction) neighboring nodes

respectively. These coefficients are calculated from an energy balance in the node, considering that heat is transferred between consecutive nodes from the central position of each node, and the resistance to heat transfer across the thickness of the node and neighboring nodes and surrounding environment in the boundary nodes. See supplementary information S1 for details on the calculation of these coefficients and the definition of the boundary conditions.

The degree of cure of the reaction was modeled by an explicit integration of the rate equation using a second order Runge–Kutta method.

In order to control the precision of the numerical integration, the process time was discretized in time steps Δt established as follows:

$$\Delta t = \min(\Delta t_{max}, \Delta t_x, \Delta t_T) \qquad (15)$$

Where Δt_{max} is the maximum allowed time step, Δt_x is the maximum allowed time step controlled by the reaction, and Δt_T is the maximum time step controlled by thermal gradients. Factors Δt_x and Δt_T were calculated before each integration step as:

$$\Delta t_x = \frac{\Delta x_{max}}{\max(dx/dt_{i,j})} \qquad (16)$$

$$\Delta t_T = \frac{\Delta T_{max}}{\max(dT/dt_{i,j})} \qquad (17)$$

Where Δx_{max} and ΔT_{max} are the maximum allowed increase of conversion and temperature respectively, dx/dt was determined from the reactive nodes, and dT/dt is calculated explicitly from the rate equation for all nodes in the system.

2.6.3 | Thermophysical models

The effective thermophysical properties of the CF reinforced composites have been calculated using models available in the literature. The longitudinal and transverse thermal conductivities have been estimated using the model reported by Struzziero and Skordos.[3] For the transverse thermal conductivity $\lambda_\perp$ (z direction) the following expression has been used:

$$\lambda_\perp = \lambda_r \cdot \left[\left(\frac{\lambda_{\perp,f}}{\lambda_r} - 1 \right) \cdot \left(\phi_f + \sqrt{\phi_f^2 - \phi_f + \frac{\left(\frac{\lambda_{\perp,f}}{\lambda_r} + 1 \right)^2}{\left(\frac{2 \cdot \lambda_{\perp,f}}{\lambda_r} - 2 \right)^2}} \right) + \left(\frac{1}{2} - \frac{\lambda_{\perp,f}}{2 \cdot \lambda_r} \right) \right] \qquad (18)$$

Where ϕ_f is the fiber volume fraction, λ_r is the resin conductivity and $\lambda_{\perp,f}$ is the transverse conductivity of the CF. In the case of the longitudinal conductivity $\lambda_{\parallel}$ (r direction):

$$\lambda_{\parallel} = \phi_f \cdot \lambda_{\parallel f} + \left(1 - \phi_f\right) \cdot \lambda_r \qquad (19)$$

Where $\lambda_{\parallel,f}$ is the longitudinal conductivity of the CF.

According to Struzziero and Skordos,[3] the transverse thermal conductivity of the CF is $\lambda_{\perp,f} = 0.84\,W/m \cdot K$, while the longitudinal conductivity $\lambda_{\parallel f} = 0.0074 \cdot T + 9.7\,W/m \cdot K$ (T in $°C$). Taking into account the experimental temperature range, an average value calculated at $60\,°C$, $\lambda_{\parallel f} = 10.14\,W/m \cdot K$ has been used.

The effective heat capacity of the composite has been estimated as:

$$c_p = w_f \cdot c_{pf} + \left(1 - w_f\right) \cdot c_{pr} \qquad (20)$$

Where w_f is the weight fraction of the CF, c_{pf} is the specific heat capacity of the CF and equal to $c_{pf} = 2.3 \cdot T + 765\,J/kg \cdot K$ (T in $°C$). An average value calculated at $60\,°C$ of $c_{pf} = 903\,J/kg \cdot K$ was used.[3]

The mass fraction of the fiber was calculated as:

$$w_f = \frac{\phi_f \cdot \rho_f}{\left(1 - \phi_f\right) \cdot \rho_r + \phi_f \cdot \rho_f} \qquad (21)$$

Where ρ_r and ρ_f are the desities of the resin and the fiber, respectively. ρ_r was estimated from the densities of the resin mixture components, as in previous works.[8] The density of the CF was obtained from the technical datasheet, with a value of $\rho_f = 1800\,kg/m^3$.

The effective composite density was calculated as:

$$\rho = \left(1 - \phi_f\right) \cdot \rho_r + \phi_f \cdot \rho_f \qquad (22)$$

Table 1 includes the values of all the thermophysical properties used in the model. It has been assumed, as a simplification, that properties do not depend on temperature nor degree of conversion, which can be considered approximately valid within the experimental range. Most of the values were obtained from different sources such as the materials libraries of the Fusion 360 software from Autodesk and Engineering Equation Solver (EES) from F-Chart software. Polyurethane foam insulation and CF properties were derived from the material data sheet and other works.[3,16] Thermophysical properties of the resin were determined from experimental data and previous studies.[8,13]

TABLE 1 Values of the thermophysical properties of the materials employed in the simulation

Material	ρ (kg/m³)	λ (W/mK)	c_P (J/kgK)
Aluminum	2700	230	897
Teflon	2150	0.28	1050
Insulation	28	0.050	2500
PLA case	1240	0.13	1800
Heating element	1380	0.17	1464
Carbon fiber	1800	0.84/10.14[a]	903
DGS4-0.45 resin	1200	0.19	1700

[a]The values of thermal conductivity correspond to the average transverse and longitudinal conductivity determined from literature data.[3]

3 | RESULTS AND DISCUSSION

3.1 | Characterization of the resin curing kinetics and properties

DGS4-0.45 formulation is an off-stoichiometric thiol-epoxy dual-curing system, in which the thiol-epoxy reaction takes place in the first curing stage, and homopolymerization of excess epoxy groups takes place in the second curing stage, using a single nucleophilic tertiary amine initiator for both reactions.[17] The sequential character of this curing process is based on both the difference in reaction kinetics and the selectivity towards the first reaction in the presence of unreacted thiol groups.[18]

The main results of the calorimetric analysis of the first and second curing stages of DGS4-0.45 formulation are given in Table 2. The reaction enthalpy of the first curing stage ($\Delta h_{\text{total},1}$) is comparable to other thiol-epoxy systems, with typical reported values within the range of 125–135 kJ/eq.[8,17] For the second reaction, the curing enthalpy ($\Delta h_{\text{total},2}$) is also comparable to the commonly reported values of 90–100 kJ/for the anionic homopolymerization of epoxy groups.[17,19] The glass transition temperature of the intermediate material (T_{gint}) is slightly below room temperature, but that of the fully cured material ($T_{g\infty}$) is clearly above room temperature and indicates that the resulting material behaves like a glassy thermoset at room temperature. Both intermediate and final T_g are in agreement with the values predicted for this family of dual-curing systems using common mixing rules.[20] With regards to the crosslinking process, it is noteworthy that the ratio between heat capacity steps of the intermediate material and unreacted formulation ($\Delta c_{Pint}/\Delta c_{P0}$) is very close to 1, which is an indication that the intermediate material is barely or not even gelled,[8] in agreement with previous studies, which

TABLE 2 Summary of the calorimetric analysis of DGS4-0.45 formulation

Summary of the calorimetric analysis of DGS4-0.45 formulation	
$\Delta h_{total,1}$ (kJ/kg)	246.6 (133.5)
$\Delta h_{total,2}$ (kJ/kg)	201.6 (87.2)
T_{g0} (°C)	−29.1
T_{gint} (°C)	14.0
$T_{g\infty}$ (°C)	91
$\Delta c_{Pint}/\Delta c_{P0}$	0.915
$\Delta c_{P\infty}/\Delta c_{Pint}$	0.542

Note: The values between brackets correspond to the reaction enthalpy in kJ/eq (kJ per Mol of reactive species).

FIGURE 4 Comparison of the experimental kinetic data at different heating rates (solid lines) with the results of the kinetic modeling (open circles): (a) first curing process, kinetic model parameters in Table 3; (b) second curing process, kinetic model parameters in Table 4 [Color figure can be viewed at wileyonlinelibrary.com]

suggested that for $f_{thiol} = 0.45$ gelation might take place at the very end of the first curing stage.[20] Indeed, one of the main purposes of the choice of such a formulation composition was to avoid gelation in the first curing stage and therefore make it possible to have a better control of the crosslinking process in the second curing stage.[8] In contrast, it is observed that for the second curing stage the ratio of heat capacity steps $\Delta c_{P\infty}/\Delta c_{Pint}$ is clearly lower than 1, which evidences the existence of a crosslinking process producing a significant reduction in network mobility due to the epoxy homopolymerization process.

Figure 4 compares the kinetics of the first and second curing process and the results of the kinetic modeling with the experimental data. It can be appreciated the radically different kinetic behavior of the first and second curing process. The kinetic data in Figure 4a reveals that the first curing process takes place at low temperatures and has a very sharp autocatalytic curing profile. In contrast, the data in Figure 4b shows that the second curing process takes place at clearly higher temperatures than the first one for all the heating rates, evidencing the sequential character of this dual-curing process.[17] An excellent agreement is also observed between the experimental data and the simulation using the model given by expressions (3) and (4) and the kinetic parameters in Table 3 (first curing process) and Table 4 (second curing process). Isothermal data was also correctly fitted by the kinetic model (Figures S1 and S2). It should be stressed that the model parameters have no connection with the reaction mechanism, they are just the result of numerical fitting of the model.

The kinetic data in Figure 4 also evidences the importance of choosing a suitable temperature program to adequately control the curing process. At 20°C, the first curing process has an apparent induction period of about
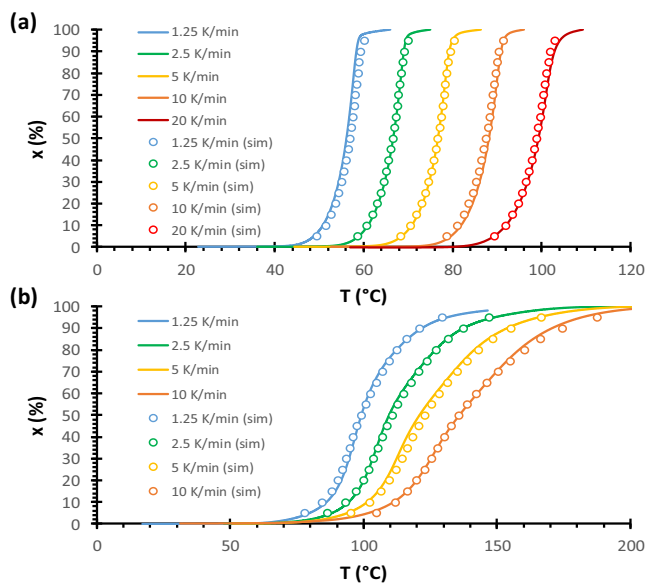
1 h and, once started, it is nearly complete in three more hours. However, at 80°C the induction period is less than 1 min and is complete in nearly 4 min overall (Figure S1). These kinetics are comparable to those reported in previous works,[8] and evidence that there is a risk of temperature overshoot in the first curing process, leading to large temperature and conversion gradients within processed parts. However, dual-curing processing somewhat simplifies the definition of the curing program, especially with regards to the choice of the first stage curing temperature,[8] taking into consideration that the curing kinetics of the second curing stage are nearly 2 orders of magnitude slower.

With regards to other relevant thermophysical properties such as thermal conductivity, density and specific heat capacity, it was decided to trust the previous results reported for similar systems and therefore use them as an approximation for the simulation of the curing process in the experimental setup. The values can be found in Table 1. This is clearly a source of uncertainty, but taking into consideration the goal and the scope of this work it is considered (a) the material properties should not differ significantly from those of a previously studied one,[8] (b) that the material would be above T_g during the whole (or most) of the curing process, and (c) that the most critical parameters are the heat release and kinetics of the curing process.

TABLE 3 Kinetic parameters of the first curing process of formulation DGS4-0.45

$\Delta h = 246600$ J/kg				
$x < x_{ind}$	E_{ind} (kJ/mol)	61.73		
	$\ln[g(x_{ind})/k_{0,ind}]$ (1/min)	-21.01		
		$i = 1$	$i = 2$	$i = 3$
$x \geq x_{ind}$	E_i (kJ/mol)	61.9	61.3	61.1
	$\ln k_{0,i}$ (1/s)	17.48	22.47	19.02
	n_i	1.602	2.506	1.625
	m_i	0.734	11.408	3.018

TABLE 4 Kinetic parameters of the second curing process of formulation DGS4-0.45

$\Delta h = 201600$ J/kg				
$x < x_{ind}$	E_{ind} (kJ/mol)	55.00		
	$\ln[g(x_{ind})/k_{0,ind}]$ (1/min)	-18.01		
		$i = 1$	$i = 2$	$i = 3$
$x \geq x_{ind}$	E_i (kJ/mol)	90.61	44.90	43.90
	$\ln k_{0,i}$ (1/s)	22.70	14.45	8.54
	n_i	4.78	8.30	1.58
	m_i	0.23	3.80	1.57

3.2 | Preliminary simulations

First of all, a number of simulations were conducted in order to establish a tentative set of process parameters that could be reasonably tested experimentally with the goal of proving the SHR concept.

The scenarios were defined taking into consideration the heating capabilities of the experimental device. According to a previous experimental characterization[11] and preliminary simulations (Figure S3), it was determined that the maximum heating rates that could be achieved were 1.5–2 and 3–4°C/min for the one-side and two-side heating 6.6 mm mold. In the case of the 15.2 mm mold, the heating rates were limited to 1–1.5 and 2–3°C/min for the one-side and two-side heating scenarios respectively. These heating capabilities are modest in comparison with the heating rates that can be achieved in the curing of thick composites,[2,21] but they are deemed sufficient for the goal of this work. Simulations predicted that the thermal lag was significantly higher for the one-side heating scenario in comparison with the two-side heating (Figure S4a). Highly uniform radial temperature profiles of the resin were also predicted by these preliminary simulations (Figure S4b), showing that the experimental device was well capable of

mimicking the one-dimensional, through-thickness heat transfer taking place in common composite processing scenarios.[2,21]

Preliminary processing simulations were carried out following temperature programs consisting of four steps: (a) A heating at a constant heating rate up to a first stage temperature, (b) an isothermal dwell at the first stage temperature, (c) a second heating up to a second stage temperature, (d) an isothermal dwell at the second stage temperature. The heating rates were fixed at 1°C/min for the one-side heated mold and at 2.5°C/min for the two-side heated mold. The first stage temperature was varied between 40 and 60°C, and the second stage temperature was fixed at 80°C. Initial temperature and environment temperature were set to 20°C.

First of all, the effect of first stage curing temperature in the two-side heated 6.6 mm mold, without filler, was analyzed. In Figure 5, it can be observed that for first stage curing temperature of 40°C there is a moderate temperature overshoot up to 70°C within the resin, and a moderate overshoot up to 45°C in the plate due to the slow dissipation of heat throughout the mold walls. When the temperature is increased to 50°C, the resin overshoot increases up to 125°C and the plate overshoot up to 57°C. However, at 60°C, there is a temperature runaway producing an overshoot within the resin up to 226°C and a plate overshoot up to 71°C. This has a direct translation into conversion profiles, as observed in Figure 5: an exceedingly high temperature overshoot leads to a premature activation of the second reaction prior to the heating up to the second stage curing temperature, leading to non-uniform conversion profiles at the end of the first stage and throughout the crosslinking process that takes place during second reaction. These simulation results are similar to those from our previous work, in which a one-dimensional heat transfer scenario was considered.[8] In consequence, a safe first stage curing temperature of 40°C may be set for the experiments in the absence of filler. In addition, the results of the simulation suggest that both the resin temperature and the
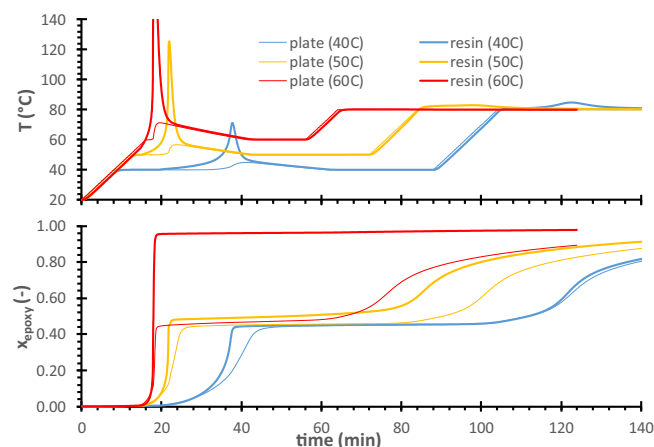
FIGURE 5 Simulated temperature (upper graph) and conversion (lower graph) profiles of the two-side heated 6.6 mm mold with different first stage temperatures (in parenthesis in the legend). In the upper graph, plate refers to the temperature of either the upper or lower plate temperature, and resin to the temperature of the innermost layer. In the lower graph, plate refers to the layer in contact with either the upper or lower plate, and resin to the innermost layer [Color figure can be viewed at wileyonlinelibrary.com]

FIGURE 6 Simulated temperature (upper graph) and conversion (lower graph) profiles of the two-side and one-side heated 6.6 mm mold with different first stage temperature of 40°C. in the upper graph, plate refers to the temperature of either the upper or lower plate temperature, and resin to the temperature of the innermost layer; upper plate and lower plate are specified for the one-side heated mold. In the lower graph, conversion is referred to the resin layers in contact with the plates or else the innermost layer (resin). The inset shows a detail of the temperature profiles simulated in the one-side heating scenario [Color figure can be viewed at wileyonlinelibrary.com]

plate temperature can be monitored in order to validate experimentally the results of the simulation.

Figure 6 compares the effect of heating on one side or both sides on the curing of 6.6 mm samples with a first stage temperature of 40°C. As already discussed, the overall curing process could be expected to be slower because of the lower heating rate that can be achieved in the one-side heating scenario. The intensity of the temperature overshoot in the first stage is somewhat lower in the one-side heated mold because of the overall lower mold temperature. When the second heating process is started, more uniform conversion and temperature profiles are obtained with the two-side heating. Unlike the two-side heated mold, two different plate temperature profiles are obtained with a single heating element on just one side (see inset). All these features can be analyzed experimentally in order to validate both the simulation model and the SHR concept.

The effect of the mold thickness and the presence of fillers was also analyzed. Figure 7 compares the temperature profiles of the two-side heated 15.2 mm mold with varying proportions of filler, using a first stage curing temperature of 40°C. It can be observed that, even if a moderate first stage temperature has been used, in the absence of fillers the accumulation of heat and the poor heat dissipation characteristics of the resin and the mold led to a thermal runaway reaching around 270°C, and a
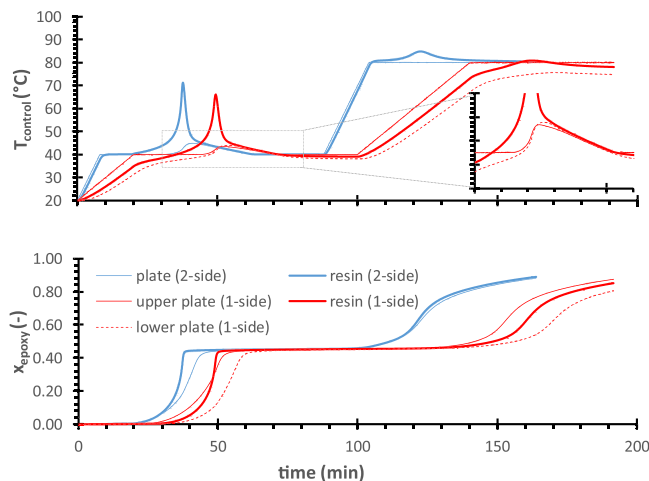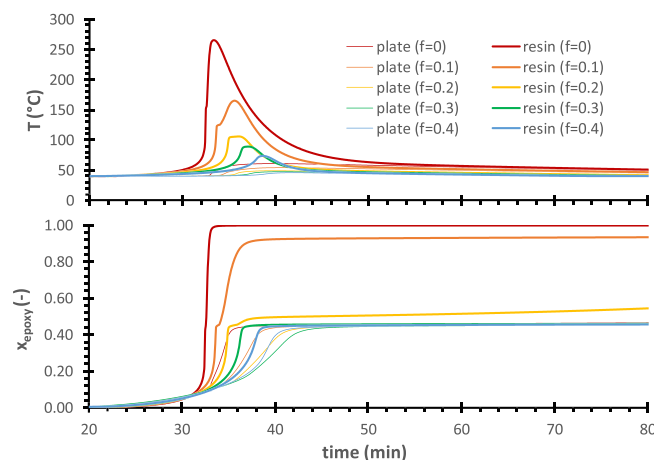

FIGURE 7 Simulated temperature (upper graph) and conversion (lower graph) profiles of the two-side heated 15.2 mm mold with different first stage temperature of 40°C and different filler content (fiber volume fraction f in the legend). In the upper graph, plate refers to the temperature of either the upper or lower plate temperature, and resin to the temperature of the innermost layer. In the lower graph, plate refers to the layer in contact with either the upper or lower plate, and resin to the innermost layer [Color figure can be viewed at wileyonlinelibrary.com]

complete loss of control of the curing sequence. As observed before, curing is almost complete within the resin, while it is only controlled and close to the expected intermediate conversion in the vicinity of the mold walls. Increasing filler content leads to a decrease in the heat evolved and a better heat management within the composite, leading to a decreasing temperature overshoot and a more controlled conversion. Indeed, it can be seen that a uniform conversion can be attained at the end of the first stage with just 30 vol% filler content.

It should be also stressed that simulations show that the experimental device can be operated safely under all the above described scenarios, due to the presence of the polyurethane foam insulation layer. This is illustrated in Figure 8, showing the temperature mapping of the mold during the processing of the one-side heated 6.6 mm sample shown in Figure 6. It can be seen that the temperature in the upper, lower and outermost layers of the mold, corresponding to the PLA casing, is always moderate, slightly higher than the environment temperature in spite of the presence of significant temperature overshoots. Indeed, the dissipation of heat from the resin to the surrounding Teflon and aluminum plates leads to moderate temperature overshoots in the aluminum

plates, which act effectively as heat sinks and slowly dissipate the excess heat to the environment. This was also observed for simulations showing temperature runaway such as those in Figure 7. Moreover, even if the aluminum plates reached temperatures higher than 80°C, the device would still be safe to operate since the PLA case temperatures would be moderate.

If one looks at the temperature distribution within the curing resin (highlighted in Figure 8 with a dashed white line), it can also be observed that the temperature gradients in the radial direction of the resin sample are also negligible due to the uniform heat distribution across the aluminum plates, with the sole exception of the sharp exothermal peak taking place during the first stage dwell ($t = 50$ min in Figure 8), where a minimal gradient is observed in the outermost layers of the sample, in the vicinity of the Teflon ring. Such gradients disappear in the subsequent heating process and activation of the second reaction ($t > = 110$ min in Figure 8). In consequence, it can be assumed that the process approaches quite well the one-dimensional heat transfer conditions usually found in RTM processing scenarios.[2,21]

Taking into account the results of all these simulations, a number of experimental tests were carried out in
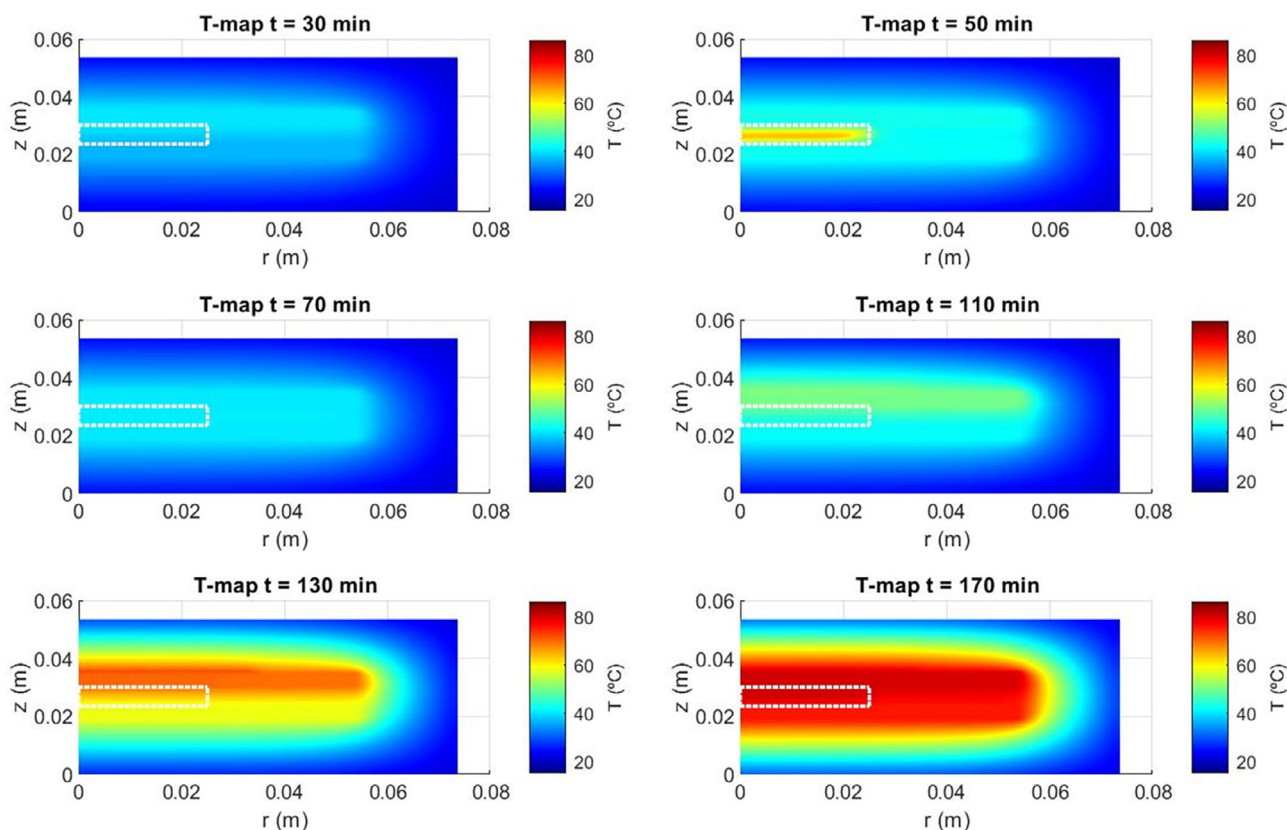

FIGURE 8 Temperature mapping of the mold obtained for the simulation of the one-side heating, 6.6 mm thickness curing scenario shown in Figure 6. The region corresponding to the resin has been highlighted with a white dashed line. Temperatures have been interpolated from simulation data using the Akima method [Color figure can be viewed at wileyonlinelibrary.com]

order to validate both the simulation model and the SHR concept. The results, their analysis and discussion are presented in the next sections.

3.3 | Experimental validation

Preliminary validation of the simulation of the one-side heating mold was already reported, using a commercially available epoxy resin.[11] The experimental temperature profiles of the upper and lower plates and the resin were correctly predicted by the simplified two-dimensional simulation model, and the effect of having a glass fiber filler was also correctly simulated.[22] In consequence, it was expected that it could also be used to validate the SHR concept making use of DGS4-0.45 formulation, taking into consideration the features of the curing process reported in the previous section, namely, (a) the sharp temperature overshoot that is obtained in the first stage curing process, (b) the monitoring of plate temperatures as a valuable method for the control of the curing process, and (c) the possibility of avoiding temperature runaway in the processing of thick composites using a suitable combination of first stage temperature and filler.

Simulations corresponding to the experimental scenarios were performed taking into account the experimental conditions: the initial temperature of the resin and the mold, environmental temperature, and the effect of the resin preparation and vacuum infusion time on the initial degree of cure of the resin when the process is started. The different scenarios analyzed experimentally are given in Table 5, along with their main characteristics. First stage and second stage dwell temperatures were fixed at 40 and 80°C/min. The heating rates employed were always 1°C/min for the one-side heating scenarios and 2.5°C/min for the two-side heating. Preparation and resin infusion time was around 30 min, but the uncertainty in the humidity/temperature conditions during preparation made it necessary to adjust the initial conversion of the first reaction in the simulations for each scenario (usually around 0.5%). The temperatures of both

upper and lower plates were monitored, in addition to the temperature at the center of the resin/composite sample and the environment temperature. Selected samples were analyzed after processing using DSC.

First of all, the scenario of the 6.6 mm mold with one-side heating only and no filler was studied (entry 1 in Table 5). The experimental results and the comparison with the results of the simulation are shown in Figure 9. In the upper graph it can be observed that the heating profiles of the resin and the plates are correctly modeled by the simulation, including the small temperature overshoot of the plates, with some logical discrepancies with the experimental results, taking into consideration the uncertainty in the preparation of the formulation and the vacuum infusion process, the values of thermophysical properties, the simplified geometrical description of the model. The most noticeable difference is the shape of the first temperature overshoot, which is experimentally broader and lower than the simulated profile. It is acknowledged that batch preparation variability is a major source of uncertainty producing variation in cure behavior, and in consequence in the intensity and position of temperature overshoots taking place during processing.[23] In the present case, sample preparation was identified as a major source of uncertainty, that is, dosage of components in the formulation (especially the initiator), homogenization, mold infusion and temperature/humidity condition. In thiol-epoxy reactions, the reaction onset and kinetics are highly sensitive to preparation conditions, the presence of catalytic impurities and storage time before analysis,[24] and the monomer feed ratio and dosage of catalyst.[18] Although it was taken care to control these factors, some uncertainty could be expected and, given the important effect on the time of the first overshoot, the initial conversion in the simulation had to be adjusted. An additional experimental issue could be the misplacement of the temperature probe within the mold, so that it would read a temperature that was closer to the upper or lower mold plates.

The simulated conversion profiles across the thickness of the resin, along the axis of symmetry, have been

TABLE 5 Summary of the different scenarios analyzed with the experimental device

Entry	Heating	Thickness (mm)	CF (vol%)	Dwell time (min, first – second)	Initial T (°C)	Room T (°C)
1	One-side	6.6	0	87–59	22	22*
2	Two-side	6.6	0	69–72	22	20
3	One-side	15.2	0	160–none	26.5	25*
4	Two-side	6.6	37	68–50	26.5	22.3
5	Two-side	15.2	29.3	90–50	25.6	22

Note: The values of room temperature marked with an * were not measured and was fixed arbitrarily for the simulations. For entry 3, only first stage was analyzed.
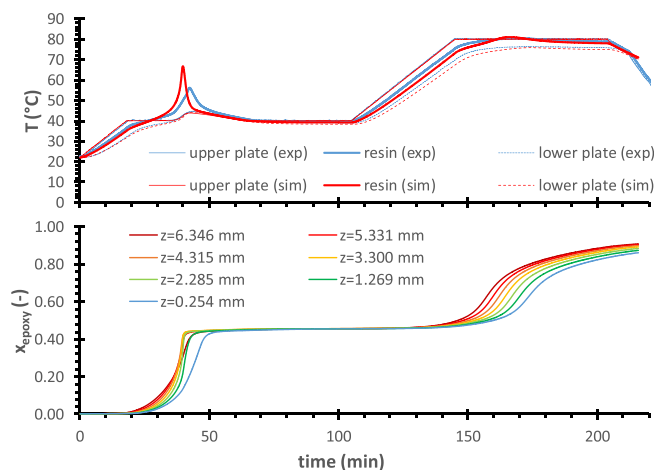
FIGURE 9 The upper graph compares the experimental and simulated temperature profiles of the curing in the one-side heated 6.6 mm mold without filler. The lower graph shows the simulated conversion profiles along the symmetry axis; the legend indicates the z position of the node, taking as $z = 0$ the lowermost layer of the sample [Color figure can be viewed at wileyonlinelibrary.com]

represented in the lower graph of Figure 9. Good separation of control of the curing stages is noticeable, leading to an almost uniform material at the end of the first stage at 40°C. Because of the temperature overshoot, conversion in the innermost layer is faster than near the mold walls, and a relevant conversion lag between uppermost (heated plate) and lowermost layers is observed. However, in spite of the uncertainty regarding the first temperature overshoot, the choice of a safe first stage temperature of 40°C ensured that premature activation of the second reaction was prevented anyway. In contrast, Figure 9 shows that when the second heating takes place and the second reaction is activated, conversion of the upper layers (closer to the heated plate) is always higher than that of the lower layers due to the existing temperature gradient between the upper and lower plates during the heating process and subsequent dwell at 80°C. As can be seen in the figure, complete conversion was not attained following this curing schedule; complete curing at 80°C or lower temperatures would have required exceedingly large processing times and it was decided to program shorter curing cycles nevertheless.

The extent of cure at the end of the first and second curing stages was analyzed experimentally. According to the simulation, the uppermost layer reached an epoxy conversion of 0.915 and the lowermost layer reached an epoxy conversion of 0.875. Assuming that the first reaction is over and considering the definition of the global conversion of epoxy groups in the preceding sections, this is equivalent to a second stage conversion of 0.845 and 0.773, respectively. The cured resin sample was removed

from the mold and was analyzed with DSC. It was found that the upper side of the sample had second stage conversion of 89%–90% (with a T_g of 77°C), which is equivalent to a global epoxy conversion of ca. 94%; the lower side of the sample had an experimental second stage conversion of 81% (with a T_g of 75°C), representing a global epoxy conversion of ca. 90%. The experimental values of conversion and T_g are consistent, taking into consideration Equation (2) and the parameters in Table 2, but they are somewhat higher than expected according to the simulation, which can be due to experimental error and also to inaccuracy of the kinetic model. The conversion of a partially processed sample, after a first stage at 40°C, was also analyzed. It was expected that the samples would have the properties of the intermediate material, with very little conversion of second stage reaction, if any. Unfortunately, the samples could not be analyzed immediately after and, given that intermediate materials are not fully stable and therefore reaction may take place slowly even at room temperature.[17] Therefore, a higher extent of cure than the theoretical 46% epoxy conversion was expected. Indeed, the sample had a second stage degree of cure of about 20% and a T_g of 25°C on both the upper and the lower sides, which is equivalent to a global epoxy conversion of ca. 57%. A similar conversion and T_g were determined in the center of the sample, evidencing that the material was uniform at the end of the first stage, as predicted by the simulation.

In addition to the temperature monitoring during processing and the DSC analyses, a visual qualitative confirmation of the state of cure and therefore the effective control of the curing sequence was obtained. Figure 10 shows some pictures of samples after the first stage and after second stage curing. The pictures evidence some of the issues encountered during experiments, such as the formation of voids coming from bubbles that could not be removed prior to infusion into the mold, or misplacement of the temperature probe (see images c and d in the figure). However, it can be observed that images a and b, that correspond to samples after first stage curing, have no color, while images c and d, that correspond to samples after second stage curing, have a uniform and intense yellow coloring. The appearance of coloring in dual-cured off-stoichiometric thiol-epoxy materials is a consequence of the occurrence of the second reaction, the epoxy homopolymerization.[20] Therefore, the absence of color in images a and b indicates that only the thiol-epoxy reaction has taken place during the first stage, as expected.

By way of contrast, the curing in the 6.6 mm two-side heated mold (entry 2 in Table 5) was also monitored and the samples were analyzed. Experimental results (not plotted) produced a temperature overshoot similar to the one predicted by preliminary simulations shown in
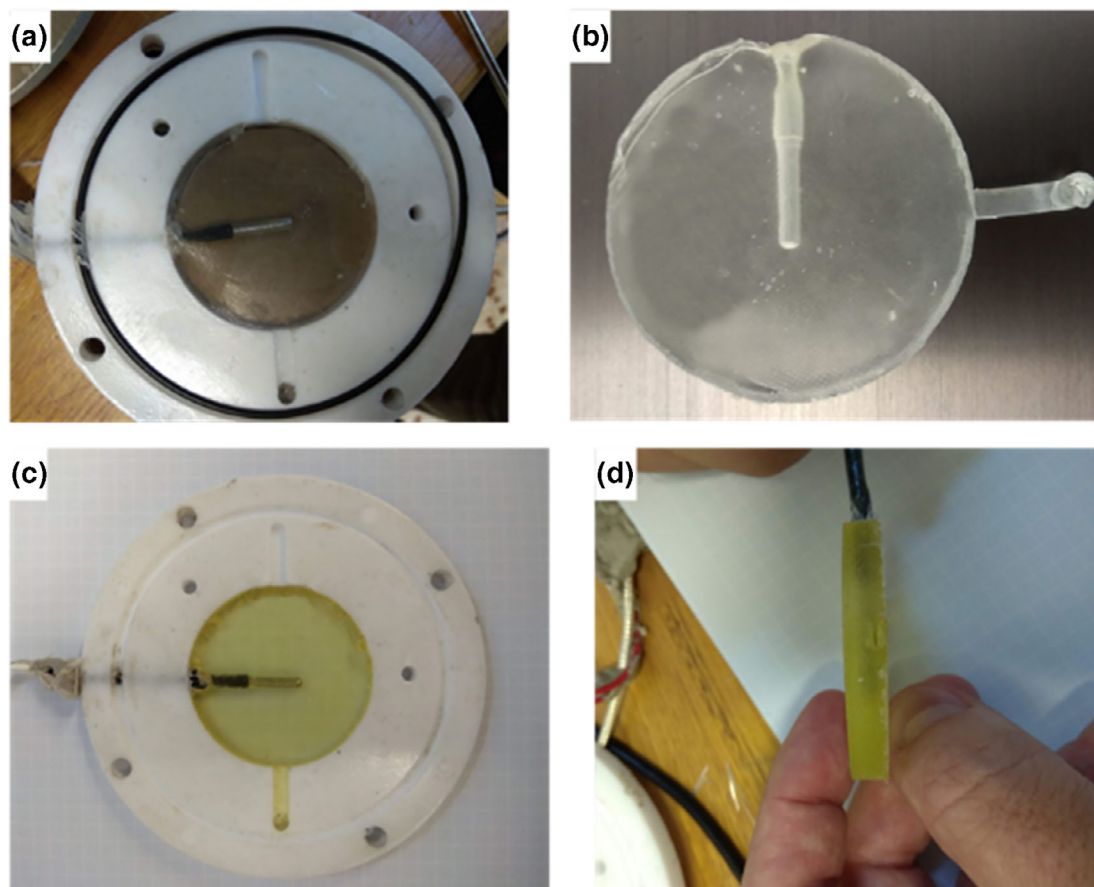
FIGURE 10 Images of samples processed in the 1-side heated 6.6 mold. (a,b) partially cured sample after first stage at 40°C. (c,d) Cured sample after first stage at 40°C and second stage at 80°C [Color figure can be viewed at wileyonlinelibrary.com]

Figure 6. Highly uniform temperature profiles during the first and second stage heating ramps, with a very small thermal lag, were also observed experimentally, in agreement with the simulation in Figure 6. When the intermediate samples were analyzed, similar problems were found due to the time elapsed between the removal of the sample from the mold and the DSC analysis. The material had a T_g of 21°C, which was somewhat above the value of 14°C for the intermediate material (see Table 2); this evidenced that, at the time of analysis, second stage conversion was about 17%, but it was uniform across the sample thickness. The material obtained after the complete process had a T_g of ca 75°C and a second stage conversion of 87%. These values agreed quite well with the temperature-conversion relationship given by Equation (2) and the parameters in Table 2. The experimental global epoxy conversion was therefore 93%, and this was in good agreement with the simulation results, yielding a second stage conversion of about 89% and a global epoxy conversion of 94%.

Next, the curing in the 15.2 mm one-side heated mold was analyzed, in the absence of fillers (entry 3 in Table 5). In the previous analysis for the two-side heated mold (Figure 7), it was observed that in the absence of fillers there would be a temperature runaway reaching up to 250–300°C. This was also to be expected in the case of the one-side heated mold, as shown in Figure 11. It can be observed that the simulation is well capable of reproducing the thermal lag during the initial heating, the height and breadth of the temperature runaway peak, the moderate temperature overshoot in both the upper and lower plates and the slow temperature decay down to the first stage temperature. The conversion profiles in the lower graph of Figure 11, corresponding to the upper half of the sample, evidence the effect of this sharp temperature runaway, leading to very fast completion of the cure process in the inner layers of the material, and a controlled extent of cure, however, at the layers in close vicinity with the upper plate. Overall, the temperature and conversion profiles are highly complex during the temperature runaway within the sample (Figures S5 and S6) due to the lack of symmetry in the z direction and the uncontrolled premature activation second reaction, leading to very high temperatures within the bulk of the sample, but more controlled in the upper and lower plates and the outer edge.
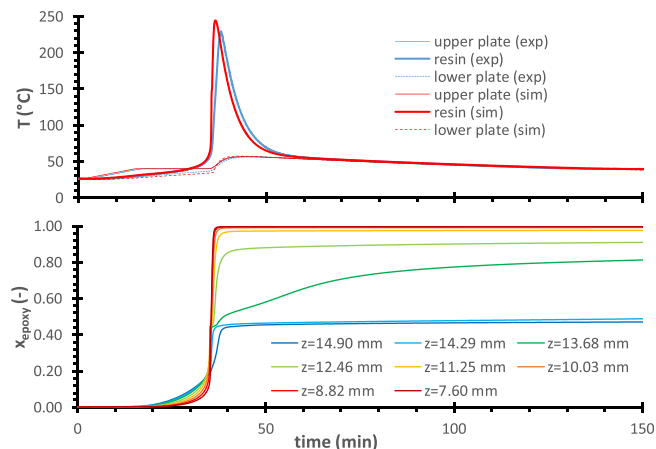
FIGURE 11 The upper graph compares the experimental and simulated temperature profiles of the curing in the one-side (upper) heated 15.2 mm mold without filler. The lower graph shows the simulated conversion profiles along the symmetry axis, but only of the upper half; the legend indicates the z position of the node, taking as $z = 0$ the lowermost layer of the sample [Color figure can be viewed at wileyonlinelibrary.com]

As a consequence, the most noticeable effect of such temperature overshoot is to produce some degradation within the material. Indeed, in Figure 12 it is observed that the processed material has a more intense coloring within, much darker than the one of the cured material under controlled conditions (see Figure 10). This is an indication of degradation taking place because of exposure to excessively high temperatures. Figure 12 shows gradient coloring in the sample, which looks lighter on the outermost layers, which is to be expected considering that heat would be dissipated through the sample boundaries to the other mold components, the Teflon ring and the plates.

This is illustrated in Figure 13, showing the simulated conversion and temperature profiles in the radial direction for the central layer of the sample. It can be seen that complete conversion is achieved except in the outermost layers, which are in contact with the Teflon ring. It is also observed the temperature and conversion profiles are very similar in the radial direction, up to a radius of
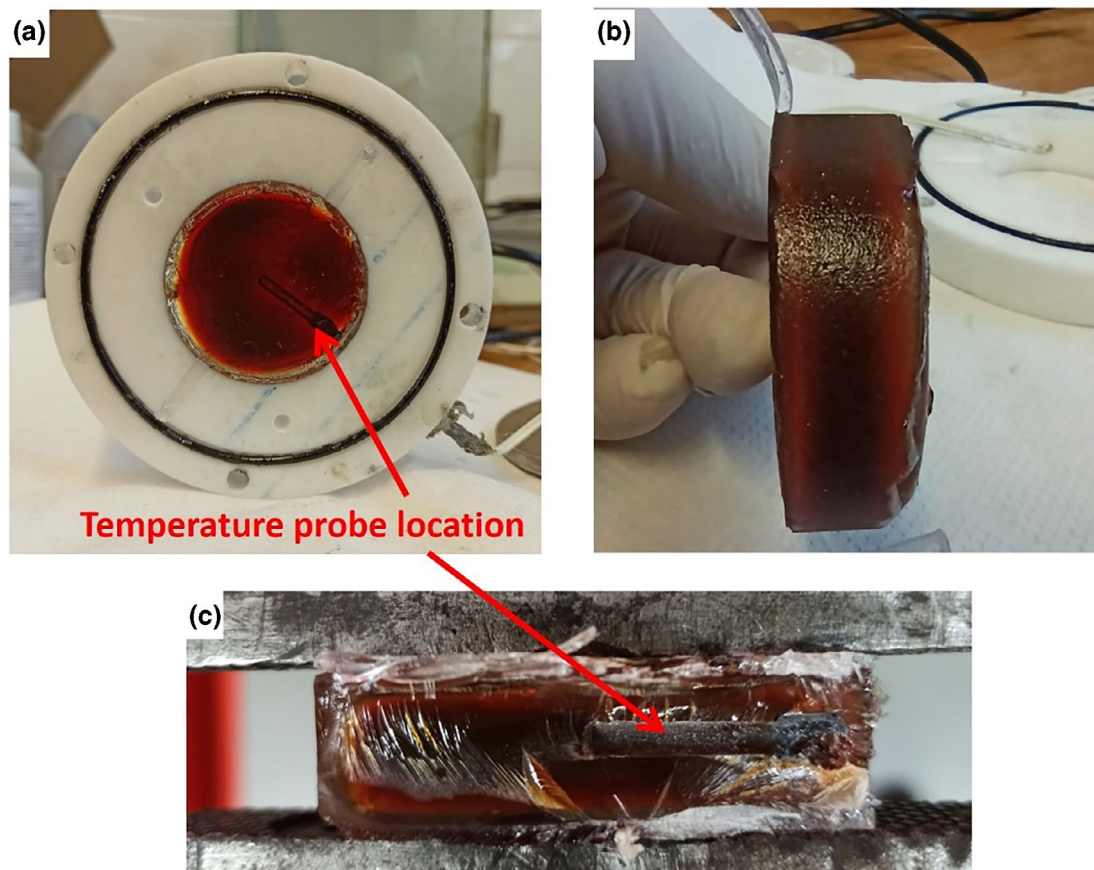

FIGURE 12 Pictures of a sample processed in the 15.2 mm mold without fillers. (a) Open mold after processing, (b) side view of the sample after removal from the mold, (c) view of the fractured surface of the sample for the removal of the temperature probe [Color figure can be viewed at wileyonlinelibrary.com]
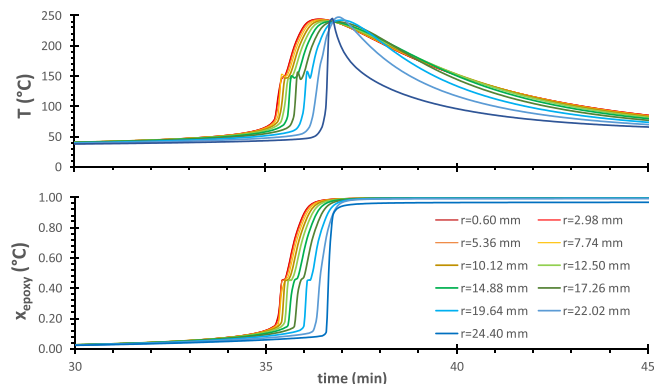
FIGURE 13 Evolution of the profiles of temperature (upper graph) and conversion (lower graph) in the central layer of the sample during processing in the one-side heated 15.2 mm mold in the absence of fillers, using a first stage temperature of 40°C. The value of $r = 0$ mm corresponds to the axis of symmetry, and the value of $r = 25$ mm to the outermost layer in contact with the Teflon ring [Color figure can be viewed at wileyonlinelibrary.com]

FIGURE 14 Experimental and simulated temperature profiles during processing of carbon-fiber filled samples in two-side heated molds of 6.6 mm (upper graph) and 15.2 mm (lower graph), using a first stage temperature of 40°C, a second stage temperature of 80°C and a heating rate of 2.5°C/min for both stages [Color figure can be viewed at wileyonlinelibrary.com]

ca. 12–15 mm and get noticeably narrower with increasing radius, especially at the outermost layers, due to the dissipation of heat to the Teflon ring, evidencing that exposure to high temperatures is very short, thereby avoiding degradation in the outermost layers. The results of the simulation contribute to explain the different coloring of the outer ring of the sample (Figure 12a. and the uppermost and lowermost layers of the material (Figure 12b,c) and serve as indirect evidence of the quality of the simulation model.

Further experimental work was carried out making use of the two-side heated mold and the incorporation of fillers. Glass fiber was attempted first, but it was seen that a negative interaction between the resin and the filler existed, leading to a very slow first curing reaction (Figure S7 in comparison with Figure 14). Such negative interaction was not observed in the analysis of conventional epoxy-amine composites.[22] This made impossible to make any comparison with the simulation results, since this effect was not accounted for in the kinetic model.

Therefore, it was decided to try CF, which apparently did not have any significant interaction with the curing system. Figure 14 shows the experimental results of samples processed in the 6.6 mm thick mold (entry 4 in Table 5, upper graph in Figure 14) and 15.2 mm mold (entry 5 in Table 5, lower graph in Figure 14). After the stage at 80°C, mold was allowed to cool down freely. Taking into consideration the amount of CF introduced in the mold before filling with the resin, the filler volume fraction was 36.4% in the 6.6 mm sample and 30.3% in the 15.2 mm sample. There was a fairly good agreement
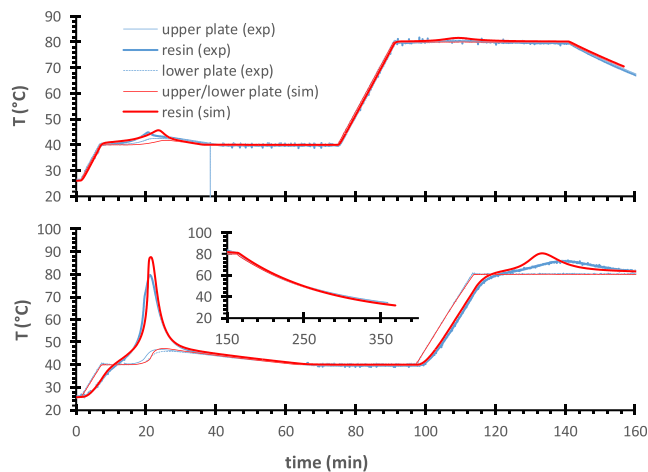
between the simulation and the experimental results. It could be verified that the mold was capable of heating at the desired heating rate of 2.5°C/min for both 6.6 and 15.2 thickness scenarios, as expected. It was also observed that the filled 6.6 mm mold had a very uniform temperature profile during the heating process, while there was a noticeable thermal lag between the plates and the resin in the 15.2 mm mold, which could be modeled successfully. In the 6.6 mm mold a tiny temperature overshoot was determined in the first stage at 40°C, while it was more relevant in the case of the 15.2 mm mold. In both cases, simulation predicted a similar behavior, showing a remarkable agreement in the 15.2 mm scenario. A second temperature overshoot in the second stage was clearly observed for the 15.2 mm sample, which could also be approximately simulated. It is also remarkable that the simulation model could also predict the cooling down of the mold at the end of the second stage (see the inset in Figure 14). The temperature and conversion profiles for the 15.2 mm scenario (Figures S8 and S9) reveals that a uniform conversion is obtained at the end of the first stage as a consequence of the controlled temperature overshoot, and that upon subsequent heating, activation of the second reaction takes place in a highly uniform way across the thickness of the sample. The high in-plane thermal conductivity of the CF greatly reduces temperature gradients and therefore conversion gradients in the radial direction (Figures S8–S11) in comparison with the non-filled scenario (Figures S5 and S6), therefore making it comparable to a one-dimensional heat transfer processing scenario.
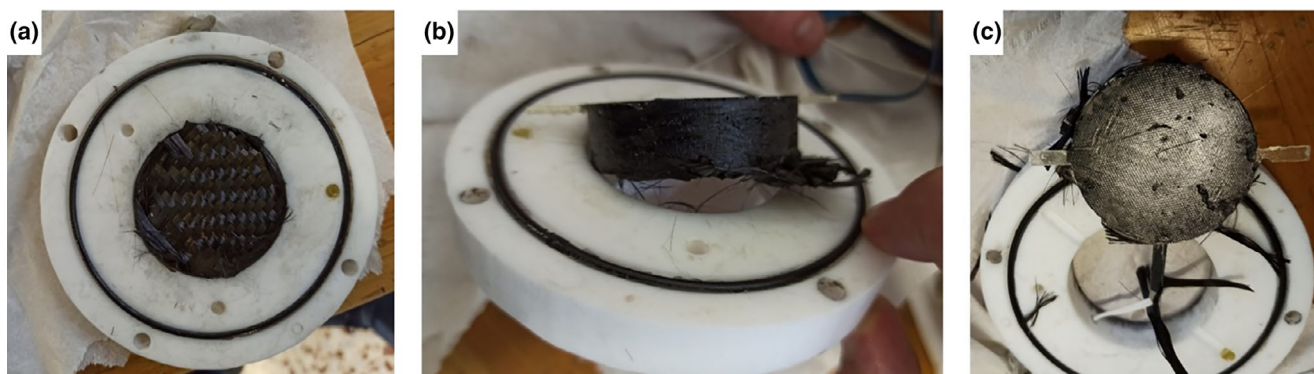
FIGURE 15 Pictures of a carbon-filled sample processed in the two-side heated 15.2 mm mold. (a) Lower view, (b) side view, and (c) upper view [Color figure can be viewed at wileyonlinelibrary.com]

Some experimental shortcomings were detected in the processing of these samples, which could influence the comparison of the simulation with the experiments. The weight of the samples was measured at the end of the process, and it was calculated that the resin volume fraction was only 48.4% for the 6.6 mm sample and 61.8% for the 15.2 mm sample, evidencing that the amount of resin infused into the mold cavity was lower than expected. This was confirmed by visual inspection of the samples after processing, as seen in Figure 15. Common defects including poor wetting of the upper/lower surface (Figure 15a,b), the outer ring (Figure 15b) or voids (Figure 15c). Other samples had similar defects. This indicates that the infusion process of the resin into mold cavity filled with CF was defective, producing voids or areas with poor wetting. Such problems were not encountered in a previous work in which the monitoring of the curing process of epoxy composites reinforced with non-woven glass fiber was studied.[22] Possible reasons are higher resin viscosity, the high filler content and the high areal weight (650 g/m^2) of the CF mat. Nevertheless, the experimental degree of cure obtained at the end of the curing processes agreed qualitatively with the predictions made with the model, taking into consideration the uncertainty in the CF content, the effect on the reaction kinetics and the model of the effective composite properties, and the effect on heat transfer within the sample.

In spite of the experimental and modeling uncertainties, the results presented in this study show that the SHR concept can be potentially used in composite processing application with the purpose of controlling the temperature gradients and overshoots during processing, therefore enabling a more uniform cure and crosslinking process leading to processed parts with higher quality. Should this particular reactive system (or a similar one) be of interest for the application in the preparation of composite parts, a more in-depth study would be necessary,

focusing on: the temperature and conversion dependence of the thermophysical properties; control of the resin viscosity for the infusion process; the effect of fillers on the reaction kinetics; effective composite thermophysical properties; the mechanical properties and the effect of processing conditions on residual stresses; the overall quality of the processed parts. Moreover, other dual-curing systems based on off-stoichiometric amine-epoxy[25] or stoichiometric dual amine-epoxy,[26] having excellent curing sequence and interesting final properties, could be easily explored in the future.

4 | CONCLUSIONS

A low-cost device for the experimental analysis of curing profiles during processing of vacuum-assisted resin transfer molding has been built. The device is capable of providing controlled heating on one or two sides of the processed sample following prescribed temperature profiles, in addition to enabling monitoring of the mold plates and resin temperatures. Samples with different thicknesses can be processed and the effect of fillers can be tested. While the capabilities of the setup are modest and some experimental issues regarding the resin infusion process need to be solved, especially for fiber-reinforced composites, the small size of the experimental device makes it suitable for the study and development of novel materials or analysis and optimization of process parameters for processing scenarios based on resin transfer molding.

The device has been successfully tested with a dual-curing formulation based on off-stoichiometric thiol-epoxy chemistry in order to validate the SHR concept. It has been shown that it is possible to control the curing sequence in the process of thick composite parts by means of choosing suitable process parameters or the use

of fillers. This can be achieved if the temperature overshoot of the first exothermic reaction can be controlled or attenuated sufficiently to prevent premature activation of the second reaction leading to large conversion and temperature gradients. Consequently, it is possible to stop the curing process at a controlled degree of conversion once the first reaction is finished, depending on the original resin formulation, making it possible to obtain a material with uniform properties.

The experimental results have been successfully simulated using a simplified geometrical definition exploiting the symmetrical design of the mold, making use of experimental kinetic data and suitable sets of thermophysical properties and effective composite model properties. This facilitates design and optimization of curing processes and allows the exploration of novel materials for composite applications in a flexible and cost-effective way.

ACKNOWLEDGMENTS

DATA AVAILABILITY STATEMENT

No. Research data are not shared.

ORCID

Xavier Fernández-Francos https://orcid.org/0000-0002-3492-2922

REFERENCES

[1] E. Ruiz, F. Trochu, *Compos. Part A Appl. Sci. Manuf.* **2006**, *37*, 913.

[2] J. L. Bailleul, V. Sobotka, D. Delaunay, Y. Jarny, *Compos. Part A Appl. Sci. Manuf.* **2003**, *34*, 695.

[3] G. Struzziero, A. A. Skordos, *Compos. Part A Appl. Sci. Manuf.* **2017**, *93*, 126.

[4] L. Sorrentino, L. Tersigni, *Appl. Compos. Mater.* **2012**, *19*, 31.

[5] X. Li, X. Han, S. Duan, G.-R. Liu, *Appl. Compos. Mater.* **2021**, *28*, 1315.

[6] V. Antonucci, M. Giordano, K.-T. Hsiao, S. G. Advani, *Int. J. Heat Mass Transf.* **2002**, *45*, 1675.

[7] D. Aleksendrić, P. Carlone, V. Ćirović, *Appl. Compos. Mater.* **2016**, *23*, 1047.

[8] M. Romero, X. Fernández-Francos, X. Ramis, *Polym. Int.* **2019**, *68*, 527.

[9] X. Ramis, X. Fernández-Francos, S. De la Flor, F. Ferrando, A. Serra, in *Thermosets: Structure, Properties, and Applications*, second ed. (Ed: Q. Guo), Elsevier, Amsterdam, Netherlands **2018**, p. 511.

[10] J. Studer, C. Dransfeld, K. Masania, *Compos. Part A Appl. Sci. Manuf.* **2016**, *87*, 282.

[11] A. Fabregat-Sanjuan, X. Fernández-Francos, F. Ferrando, in *Actualidad de la Ingeniería Mecánica en Iberoamérica* (Ed: M. J. del Martínez), Publicaciones UIS, Bucaramanga, Colombia **2019**.

[12] K. N. Marsh Ed., *Recommended Reference Materials for the Realization of Physicochemical Properties*, Blackwell Scientific Publications, Oxford, England **1985**.

[13] J. M. Hutchinson, F. Roman, P. Cortes, Y. Calventus, *Polimery* **2017**, *62*, 560.

[14] R. A. Venditti, J. K. Gillham, *J. Appl. Polym. Sci.* **1997**, *64*, 3.

[15] E. Frulloni, M. M. Salinas, L. Torre, A. Mariani, J. M. Kenny, *J. Appl. Polym. Sci.* **2005**, *96*, 1756.

[16] D. S. W. Pau, C. M. Fleischmann, M. J. Spearpoint, K. Y. Li, *Fire Mater.* **2014**, *38*, 433.

[17] X. Fernández-Francos, A.-O. Konuray, A. Belmonte, S. De la Flor, À. Serra, X. Ramis, *Polym. Chem.* **2016**, *7*, 2280.

[18] A. O. Konuray, X. Fernández-Francos, X. Ramis, *Polym. Chem.* **2017**, *8*, 5934.

[19] S. K. Ooi, W. D. Cook, G. P. Simon, C. H. Such, *Polymer* **2000**, *41*, 3639.

[20] A. Belmonte, X. Fernández-Francos, À. Serra, S. De la Flor, *Mater. Des.* **2017**, *113*, 116.

[21] E. Ruiz, F. Trochu, *Compos. Part A Appl. Sci. Manuf.* **2005**, *36*, 806.

[22] A. Fabregat-Sanjuan, X. Fernández Francos, F. Ferrando-Piera, in *Anales de Ingeniería Mecánica Revista de la Asociación Española de Ingeniería Mecánica* (Ed: X. C. N. I. de Mecánica), AEIM, Jaén **2021**.

[23] T. S. Mesogitis, A. A. Skordos, A. C. Long, *Compos. Sci. Technol.* **2015**, *110*, 145.

[24] R. M. Loureiro, T. C. Amarelo, S. P. Abuin, E. R. Soulé, R. J. J. Williams, *Thermochim. Acta* **2015**, *616*, 79.

[25] A. O. Konuray, N. Areny, J. M. Morancho, X. Fernández-Francos, À. Serra, X. Ramis, *Polymer* **2018**, *146*, 42.

[26] O. Konuray, A. García, J. M. Morancho, X. Fernández-Francos, À. Serra, F. Ferrando, M. García-Alvarez, X. Ramis, *Eur. Polym. J.* **2019**, *116*, 222.

SUPPORTING INFORMATION

Additional supporting information may be found in the online version of the article at the publisher's website.

How to cite this article: A. Fabregat-Sanjuan, X. Fernández-Francos, F. Ferrando-Piera, *J. Appl. Polym. Sci.* **2021**, e52009. https://doi.org/10.1002/app.52009